

## A model for simulating deepwater oil and gas blowouts – Part I: Theory and model formulation

### Un modèle pour simuler les éruptions en eau profonde de pétrole et de gaz – Partie I: Formulation de la théorie et du modèle

LI ZHENG, *Research Associate, Department of Civil and Environmental Engineering, Clarkson University, Potsdam, NY 13699, USA (now at Quantitative Environmental Analysis, Montvale, NJ 07645, USA)*

POOJITHA D. YAPA, *Professor, Department of Civil and Environmental Engineering, Clarkson University, Potsdam, NY 13699, USA*

FANGHUI CHEN, *Graduate Research Assistant, Department of Civil and Environmental Engineering, Clarkson University, Potsdam, NY 13699, USA*

#### ABSTRACT

A model developed to simulate the behavior of oil and gas accidentally released from deep water is presented. This model presents major modifications to a three-dimensional model developed earlier (Yapa and Zheng, 1997) that simulate the behaviour of oil from under water accidents (shallow water). In deepwater, the ultra-high pressure and cold temperature causes phase changes in gases. These combined with relatively strong currents in some deepwater regions presents extraordinary challenges to modeling jets/plumes from deepwater oil and gas blowouts. The present model incorporates the phase changes of gas, associated changes in thermodynamics and its impact on the hydrodynamics of the jet/plume. Hydrate formation, hydrate decomposition, gas dissolution, non-ideal behavior of the gas, and possible gas separation from the main plume due to strong cross currents are integrated with the jet/plume hydrodynamics and thermodynamics.

This paper presents the complete model development and testing of various computational modules with available data. A companion paper presents the comparison of model results with three large-scale field experiments conducted in the Norwegian Sea.

#### RÉSUMÉ

On présente un modèle développé pour simuler le comportement de pétrole et de gaz accidentellement libérés en eau profonde. Ce modèle présente des modifications majeures par rapport à un modèle tridimensionnel développé précédemment (Yapa et Zheng, 1997) qui simulait le comportement de l'huile suite à des accidents sous-marins (en eau peu profonde). En eau profonde, les très fortes pressions et la température froide provoquent des changements de phase en gaz. Ceux-ci combinés avec les courants relativement forts dans certaines régions en eau profonde constituent un réel défi pour modéliser les jets et panaches des éruptions de pétrole et de gaz en eau profonde. Le modèle actuel incorpore les changements de phase en gaz, les changements associés de la thermodynamique et leur impact sur l'hydrodynamique du jet/panache. La formation et décomposition d'hydrate, la dissolution de gaz, le comportement non-parfait du gaz, et la séparation possible de gaz du panache principal due aux forts courants en travers, sont intégrés à l'hydrodynamique et la thermodynamique du jet/panache.

Cet article présente le développement complet du modèle et les tests de divers modules informatiques avec des données disponibles. Il est accompagné d'un autre article qui fait la comparaison des résultats du modèle avec trois expériences à grande échelle conduites sur le terrain en Mer de Norvège.

**Keywords:** Blowout models; deepwater spills; deepwater models; oil spills; oil and gas spills; gas hydrates; well head blow outs; underwater blowouts.

#### 1 Introduction

Steadily increasing oil and gas exploration and production from deepwater locations (water depths in excess of 300 m) are found in several regions in the world: e.g. Gulf of Mexico, the North Sea, off shore West Africa, and off shore Brazil. According to Lane and Labelle (2000), the number of exploratory wells in the Gulf of Mexico (GOM) has increased by 70% from 1996 to 1998. They estimate the production from installations deeper than 800 m to be 69% of the total production by year 2007. The oil industry plans to extend the exploration and production from

as deep as 3000 m water depth. As the production increases the potential for an oil/gas spill increases. Major concerns from a deepwater oil/gas spill are fire, toxic hazard to the people working on the surface installations, and loss of buoyancy of ships and any floating installations. Therefore, it is important to know when, where, and how much gas will surface. Another environmental concern is whether oil will surface and if so, where, when, and what the oil slick thickness be. To meet these new challenges, spill response plans need to be upgraded. An important component of such a plan would be a model to simulate the behavior of oil and gasses, if accidentally released, in deepwater.

Revision received March 20, 2002. Open for discussion till December 31, 2003.

Figure 1 schematically shows a scenario of a deepwater oil/gas blowout. Initially, spilled oil/gas mixture rises as a jet/plume (near-field phenomena), which may gradually lose its momentum and buoyancy due to the entrainment of ambient fluid in a stratified ocean environment. Gas expands as it rises because of the pressure drop and thus increases the buoyancy of the jet/plume. Under field conditions, oil and gas are known to move as individual droplets (far-field conditions) beyond the neutral buoyancy level (Rye *et al.* 1997; Yapa *et al.*, 1999). Whether a jet/plume reaches the neutral buoyancy level below the water surface depends on a number of factors such as ambient stratification, density of oil, depth of release, and the velocity of release.

A deepwater blowout differs from those in shallow water in several aspects:

- i. Under high pressure and low temperature, gas may be converted to a solid like phase called gas hydrate. Gas hydrates consist of gas and water, and is a slush like (similar to frazil ice) compound. For CH<sub>4</sub>, the formation of hydrate can be described as follows.

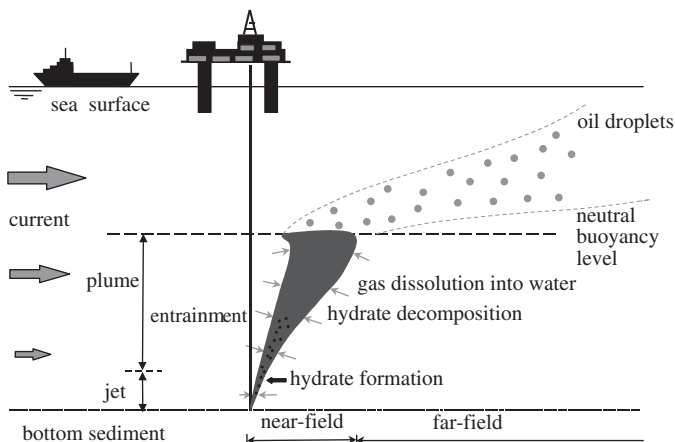
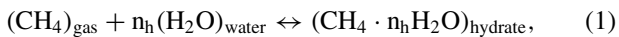


Figure 1 Problem description.

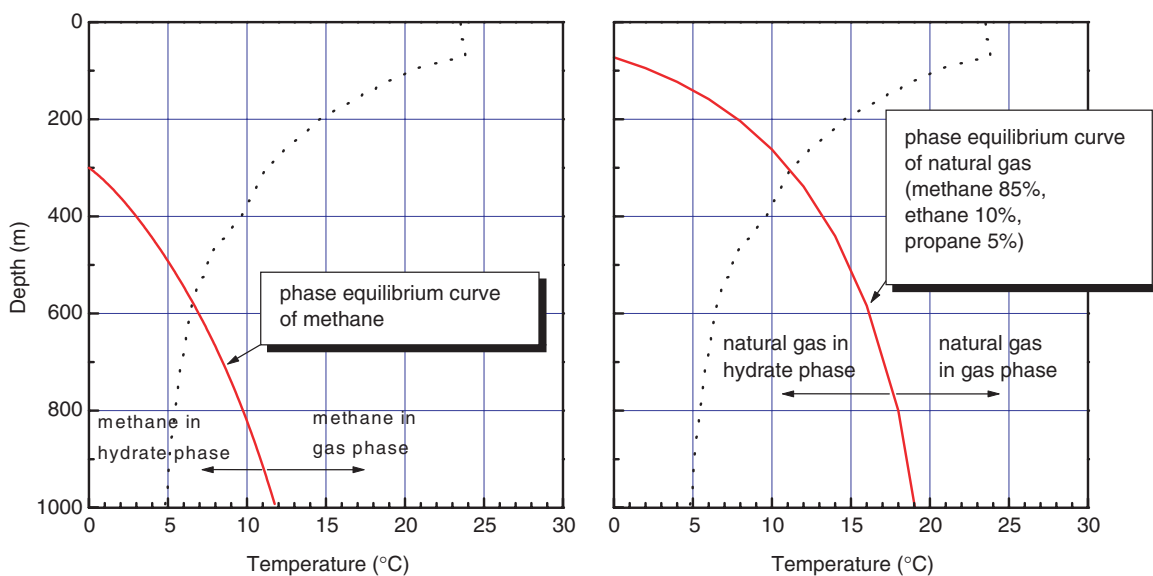


Figure 2 Hydrate phase equilibrium diagrams for CH<sub>4</sub> (a) and natural gas (b) superimposed on temperature distribution at a location in the Gulf of Mexico.

in which  $n_h = 5.75$  for CH<sub>4</sub>. As a jet/plume rises to a level of lower pressure, hydrate may decompose into water and gas again. Figure 2a and b shows water temperature variation (dotted line) and the thermodynamic equilibrium conditions (solid line) for CH<sub>4</sub> (Figure 2a) and natural gas (Figure 2b) at a location in GOM. Below the solid line, the pressure and temperature satisfy the hydrate formation conditions. Above the solid line, hydrates will begin to decompose. At this location, the thermodynamic conditions for forming hydrates will be met around a depth of 500 m for CH<sub>4</sub> and 250 m for natural gas. Hydrate formation and decomposition significantly affects buoyancy of the jet/plume.

- ii. Free gas may dissolve into water during its long journey and thus change the buoyancy of the jet/plume as well.
- iii. Under high pressure, gas behaviour is better described by a non-ideal gas state equation instead of an ideal one.
- iv. Size of gas bubbles and their buoyant velocities (or slip velocities) can no longer be approximated as constant, considering the processes of gas hydrate formation, decomposition, gas dissolution, and gas expansion.
- v. Gas may escape from a jet/plume due to the gas bubble slip velocity if the jet/plume is significantly bent in a cross flow.

Yapa and Zheng (1997) detailed a model for simulating oil spills from underwater accidents. Their model could also simulate the presence of gas with oil for relatively vertical jets/plumes. Part II of their paper (Zheng and Yapa, 1998) compared the model simulations in detail with numerous laboratory data and a few small-scale field experiments that used compressed air. In all cases, the model simulation compared well with observed data. Later a modified version of this model was used to compare the results from two field experiments. The two field experiments, conducted in the Norwegian sea by SINTEF (Norway), consisted of oil and gas releases at around 100 m depth (Rye *et al.*, 1997). The experimental data were unique because of the logistical and legislative difficulties in conducting field experiments of oil spills and the large costs associated with them. The comparisons of their

model simulations with SINTEF experiments were given in Yapa *et al.* (1999).

Yapa and Zheng's (1997) model, is not suitable for applications in deepwater because of major differences in gas behavior when compared to relatively shallow water. These differences were explained in detail earlier. The existence of strong currents in some deepwater regions (e.g. GOM) as reported by Cooper *et al.* (1990) can cause gas phase to separate from the oil/gas plume. This is another reason why the previous model needed major modification. Yapa *et al.* (2001) coupled a module for hydrate formation and decomposition with their former model (Yapa and Zheng, 1997) to calculate several scenarios of deepwater blowouts. Johansen (2000) developed a comprehensive deepwater spill model capable of simulating gas hydrate formation/decomposition, gas dissolution, and gas separation from the main plume. The simulations for hydrate formation/decomposition in Johansen (2000) were based on thermodynamics only. The reaction rates of formation and decomposition (i.e. kinetics) were ignored. The model reported by Yapa *et al.* (2001) was written during the middle stages of the project and it did not include the complete model formulation or the comparisons with "Deepspill" field experiment data (Johansen *et al.*, 2001). Spaulding *et al.* (2000) reported a deepwater model which could simulate hydrate formation. No details were provided in Spaulding *et al.* (2000) regarding the hydrate formation calculation. Barbosa *et al.* (1996) and Topham (1984a,b) integrated an empirical hydrate formation developed by Vysniauskas and Bishnoi (1983) with a plume model to simulate deepwater blowout scenarios. None of the papers referred above compared field data (none available at that time) with model simulations.

This paper describes the development of a mathematical model to simulate the behavior of oil and gas released from deepwater and simulations using the model. The model formulation integrates hydrodynamics and thermodynamics of the jet/plume, the thermodynamics and kinetics of hydrate formation and decomposition, and gas dissolution. The model uses an improved integrated formulation for computing buoyant velocity of gases and hydrates. The model also uses an improved integrated formulation to compute dissolution that gives good results even in deepwater conditions, where the behavior of gas may not be ideal. The model can simulate the behaviour of oil and gas in strong cross flow conditions where gases may separate from the main plume. Each module was tested by comparing the computational results with available data. Some of these cases are presented in this paper. The integrated model will be referred to as CDOG for convenience. In part II (the companion paper by Chen and Yapa, 2003), CDOG is used to simulate and compare the results with large scale field experiments, "Deepspill".

## 2 Kinetics of hydrate formation and decomposition

### 2.1 Previous work on hydrates

Studies on gas hydrates were summarized in detail by Holder *et al.* (1988) and Sloan (1997). These studies could be broadly divided

into two categories: thermodynamics and kinetics. Thermodynamic studies focus on the conditions of hydrate formation, such as equilibrium temperature and pressure. Kinetic studies focus on the rate of formation and decomposition. The existence of hydrates depends on not only the thermodynamics but also the kinetics of formation. Our computations showed that the time for a gas bubble to completely convert to hydrate is sometimes of the same order of magnitude as the time for a plume to rise to neutral buoyancy level. Therefore, hydrate kinetics are included in the present model. Vysniauskas and Bishnoi (1983) proposed the first kinetic hydrate formation theory, a semi-empirical model for the gas consumption rate. Englezos *et al.* (1987a,b) developed an intrinsic kinetic model for hydrate growth. This intrinsic model was then extended to an electrolyte solution (Dholabhai *et al.*, 1993) and applied to hydrate plugging problems in under-sea natural gas pipelines under shutdown conditions (Jamaluddin *et al.*, 1991).

Research on gas bubble hydrate formation and decomposition is limited when compared with the work to avoid plugging in natural gas pipelines caused by hydrate formation. Maini and Bishnoi's (1981) experiments investigated the hydrate formation of gas bubbles in 3°C water under different pressures. They found that a layer of hydrate coating (or shell) was formed at the surface of gas bubbles when the pressure was 4826 kPa or higher. Shedding of small hydrate particles from the edges of the bubbles was also observed. Topham (1984a) argued that the hydrate was formed at the outer surface of hydrate shell and gas is brought from inside the shell by the capillary action. Based on experimental observations and theoretical evaluations, Gumerov and Chahine (1998) concluded that the hydrate formation of gas bubbles was controlled by the heat transfer rather than mass diffusion. Brewer *et al.*'s (1998) field experiments investigated the hydrate formation of CH<sub>4</sub> and CO<sub>2</sub> in deep sea. They observed that the period for the hydrate nucleation was very short for these gases in deep sea. Johansen (2000) integrated the models of hydrate formation and decomposition, which were based on the thermodynamics, with a plume model to simulate the deepwater spills.

### 2.2 Integrating hydrate formation kinetics with mass and heat transfer

To model the hydrate formation rate in the gas phase of the jet/plume, three processes need to be considered: hydrate kinetics, mass transfer, and heat transfer. Mass transfer transports gas for hydrate formation to the point of reaction. Heat transfer re-distributes the heat released from hydrate formation around the solid hydrate to change the water temperature. No previous research has taken into account all of the above three processes when simulating the hydrate formation in a deepwater gas plume. In this paper, the method of Englezos *et al.* (1987a) for hydrate kinetics is integrated with the mass and heat transfer phenomena to model the hydrate formation.

Before integrating the hydrate kinetics with the hydrodynamics and thermodynamics of jet/plume, a module is constructed

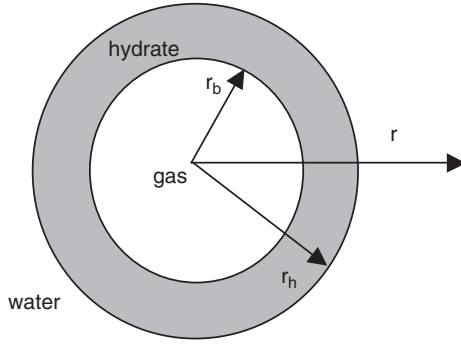


Figure 3 A schematic diagram of a gas bubble with a hydrate shell.

to check the correctness of adaptation and numerical algorithms. We will refer to this as the module for hydrate kinetics.

The module described in this section is for a single gas bubble in infinite water. In the jet/plume model the same methodology is applied to multiple gas bubbles. The module includes thermodynamics of hydrate formation. The nucleation process is neglected because experimental observations (Maini and Bishnoi, 1981; Bishnoi and Natarajan, 1996; Brewer *et al.*, 1998) show that this period is very short. Since the actual gas bubbles may not be exactly spherical, the reference to gas bubbles should be interpreted as volume-equivalent spheres. Figure 3 shows a schematic diagram of a single gas bubble with hydrate coating.

The Following assumptions are made for this module.

- (i) Mass transfer: Gas molecules diffuse through the porous hydrate shell due to the concentration gradient of gas, and react with water to form hydrates at the hydrate-water interface.
- (ii) Heat transfer: The hydrate shell is at the same temperature as the hydrate-water interface. The heat released due to hydrate formation at the hydrate-water interface is transferred only through the water phase, since the gas phase thermal conductivity is much less than that of the liquid phase.
- (iii) Both gas mass and heat transfers are considered to be quasi-steady, i.e. the transfer of mass and heat at any cross-section is the same for a given time. This assumption implies a slowly moving boundary for gas bubbles, which is met by implementing a small time step  $\Delta t$ .
- (iv) The pressure between inside and outside the bubble are equal. The porous nature of the hydrate shell that separates the gas and liquid is thought to justify this.
- (v) Any shedding hydrate particles from the edges of bubbles are not taken into account in the computations and the hydrate shell homogeneously covers the bubble surface.

#### Kinetics of hydrate formation

Englezos *et al.* (1987a) describes the rate of hydrate growth as:

$$\frac{dn}{dt} = K_f A (f_{dis} - f_{eq}) \quad (2)$$

in which  $dn/dt$  = gas hydrate formation rate [mol/s];  $A$  = hydrate formation surface area [ $m^2$ ] =  $4\pi r_h^2 \psi_s$ ;  $\psi_s$  = an overall shape factor to accommodate the non-spherical shape;  $K_f$  = hydrate formation rate constant [mol gas/ $m^2 \cdot MPa \cdot s$ ], the

values of  $K_f$  for  $CH_4$  and  $C_2H_6$  (ethane) were given in Englezos *et al.* (1987a);  $f$  = fugacity [MPa]; subscripts “dis” and “eq” represent the values of dissolved gas and at three-phase equilibrium condition, respectively. Fugacity can be viewed as the equivalent of partial pressure for non ideal gases.  $f_{eq}$  is computed by using the method described by Sloan (1997).  $f_{dis}$  is computed using Henry’s law. More details on this computation can be found in Yapa *et al.* (2001).

#### Mass transfer rates

The quasi-steady diffusion equation and boundary conditions in the hydrate zone are:

$$\frac{d}{dr} \left( r^2 \frac{dC}{dr} \right) = 0 \quad r_b \leq r \leq r_h \quad (3)$$

$$C(r_b) = C_0 \quad (4)$$

$$C(r_h) = C_i \quad (5)$$

$$-D_g 4\pi r_h^2 \psi_s \left. \frac{dC}{dr} \right|_{r=r_h} = \frac{dn}{dt} \quad (6)$$

in which  $C$  = gas concentration [mol/ $m^3$ ];  $D_g$  = effective diffusion coefficient [ $m^2/s$ ];  $C_i$  = value of  $C$  at the hydrate-water interface,  $C_i$  varies with the rate of hydrate formation;  $C_0$  = value of  $C$  at the hydrate-gas interface;  $r_b, r_h$  = radii of gas bubble and hydrate shell, respectively.

#### Heat transfer rates

The quasi-steady diffusion equation and boundary conditions in the water zone are:

$$\frac{d}{dr} \left( r^2 \frac{dT}{dr} \right) = 0 \quad r \geq r_h \quad (7)$$

$$T(r_h) = T_i \quad (8)$$

$$T(\infty) = T_\infty \quad (9)$$

$$-K_w 4\pi r_h^2 \psi_s \left. \frac{dT}{dr} \right|_{r=r_h} = \lambda \frac{dn}{dt} \quad (10)$$

in which  $T$  = Temperature [K];  $T_i$  = temperature at the hydrate-water interface [K] – varies with the rate of hydrate formation;  $T_\infty$  = water temperature before hydrate formation [K];  $K_w$  = thermal conductivity of water [W/ $m \cdot K$ ];  $\lambda$  = latent heat of hydrate formation [J/mol gas].

#### Size of gas bubble

Using non-ideal gas law, the state variables can be related as:

$$P_\infty \frac{4}{3} \pi r_b^3 = n Z R T_\infty \quad (11)$$

in which  $P_\infty$  = hydrostatic pressure of surrounding water [MPa];  $n$  = number of moles;  $Z$  = the compressibility factor; and  $R$  = the universal gas constant = 8.31 [J/mol  $\cdot$  K].

### 2.3 Kinetics of hydrate decomposition

Kim *et al.* (1987) expressed the rate of decomposition for hydrate using an equation similar to Eq. (2). The main differences are the fugacity terms now being reversed,  $f_g^v$ , fugacity of gas at the particle surface temperature and the pressure of surrounding water

replacing  $f_{dis}$ , and the kinetic rate constant being an exponential function of the hydrate particle surface temperature. The details of this formulation were given in Yapa *et al.* (2001).

A series of numerical tests revealed that the results from the model with heat transfer process coupled with the kinetics of hydrate decomposition are very close to those achieved without the heat transfer process. Therefore, for simplicity, the effect of heat transfer during the hydrate decomposition is ignored. The temperature at the hydrate particle surface is assumed to be the water temperature.

#### 2.4 Verification of the hydrate module using experimental data

In the absence of extensive experimental data specifically for the hydrate formation of gas bubbles, the best check for the model is to compare the model results with experimental data from similar tests. The laboratory experimental data from Jamaluddin *et al.* (1991) for the hydrate slab growth (1-D) are chosen here, because the mechanism of hydrate slab growth is the same as that of a gas bubble hydrate formation. Moreover, these data can be considered reliable because experimental conditions for hydrate slab growth in the laboratory are easier to control than those for gas bubble hydrate formation. No quantitative information is available for the gas bubble hydrate formation in a jet/plume under field conditions. The governing equations of the present model for gas bubbles in spherical coordinates can be converted to those for hydrate slab growth.

Numerically simulated hydrate surface temperature and CH<sub>4</sub> consumption with respect to time compared very well with the observed data and was presented in Yapa *et al.* (2001). The latter comparison is repeated here in Figure 4 to show the comparison of CH<sub>4</sub> consumption at two different pressures. Both cases show good comparison with observed data. The results from the present model are very close to those from Jamaluddin *et al.* (1991) using an unsteady model. However, the quasi-steady approach used in this paper does not require discretization of the governing equations in space domain. Hence, the computational time is reduced significantly.

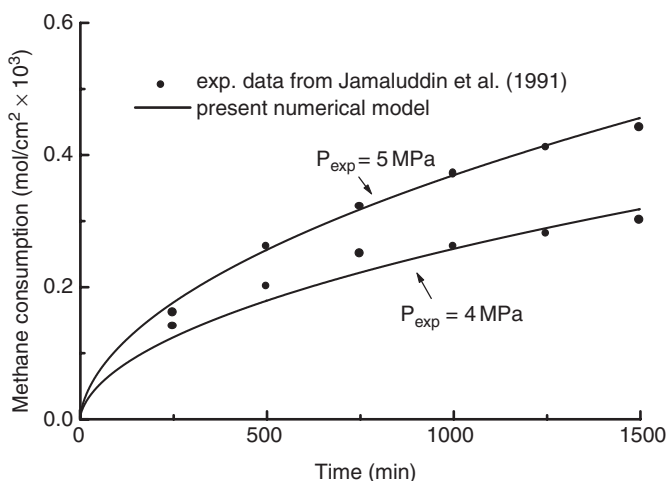


Figure 4 Effect of pressure on methane gas consumed to form hydrates ( $T_{exp} = 274$  K).

#### 2.5 Setting parametric constants for gas hydrate formation

Topham (1984a) used Maini and Bishnoi's (1981) measured bubble life time of 180 s in his model calibration. This is the only published data we found for the hydrate formation for a gas bubble. Our simulations using  $\psi_s = 38$  gives a bubble life of 178 s. This  $\psi_s$  value will be used for all simulations in CDOG model.

No experimental data are available on the effective diffusion coefficient  $D_g$ . Considering the characteristics of a cracked shell,  $D_g$  in the hydrate shell is expected to be greater than that in a hydrate slab or other stable hydrate body. Numerical tests conducted showed that the model results are not sensitive to  $D_g$  if  $D_g \geq 1 \times 10^{-6}$  m<sup>2</sup>/s.  $D_g = 1 \times 10^{-6}$  m<sup>2</sup>/s is used for all simulations. Detailed discussion on diffusion coefficient to be used in hydrate simulations can be found in Chen and Yapa (2001b).

### 3 Dissolution of gases in deepwater plumes

#### 3.1 Previous work on gas dissolution

In models that considered the gas dissolution, the dissolution mass transfer rate was computed using the simple Henry's law. In deepwater, the solubility is affected by high pressures. The dissolution computed by using simple Henry's law deviates significantly from the actual values in ultra-high pressure conditions.

In general, the dissolution mass transfer rate  $dm/dt$  for a gas bubble is calculated by

$$\frac{dm}{dt} = KMA(C_s - C_0) \quad (12)$$

where  $m$  = mass of a gas bubble [kg];  $K$  = mass transfer coefficient [m/s];  $M$  = molecular weight of gas [kg/mole];  $A$  = surface area of a gas bubble [m<sup>2</sup>];  $C_0$  = concentration of dissolved gas [mole/m<sup>3</sup>];  $C_s$  = saturated value of  $C_0$  (i.e. solubility).

The major parameters in Eq. (12) are the solubility  $C_s$  and mass transfer coefficient  $K$ . Liro *et al.* (1992) adopted a constant solubility for CO<sub>2</sub> in water. Wuest *et al.* (1992) used the simple Henry's law to calculate the oxygen solubility in water, which is appropriate for shallow water but not suitable for deepwater. In the same paper Wuest *et al.* (1992) calculated the mass transfer coefficient using a correlation based on small size oxygen bubbles. Drange and Haugan (1992), and Johansen (2000) calculated the mass transfer coefficient using formulations for spherical rigid and fluid particles, respectively. The effect of salinity on CO<sub>2</sub> solubility was considered by Drange and Haugan (1992).

The solubility may be affected by the salinity and temperature in the seawater. The effects of high pressure, the temperature, and the salinity on gas solubility and the computation of mass transfer coefficient are discussed in the next two sections.

#### 3.2 Non-ideal behavior of gas in deepwater

In deepwater, the behavior of gas is non-ideal due to high ambient pressure. The solubility of gas in water is strongly dependent on the ambient pressure, temperature, and salinity. Gas bubbles may

experience significant variations in sizes and shapes because of gas expansion and dissolution. Therefore, ways of estimating solubility and mass transfer coefficient need to be improved. The deviation of a real gas from the ideal gas can be described by the compressibility factor  $Z$ :

$$Z = \frac{PV}{nRT} \quad (13)$$

where  $P$  = ambient pressure;  $V$  = gas volume;  $n$  = number of moles of gas;  $R$  = universal gas constant;  $T$  = ambient temperature. For an ideal gas,  $Z \equiv 1$ .

Figure 5 shows the temperature profile for a location in the Gulf of Mexico and the  $Z$  values for  $\text{CH}_4$ ,  $\text{CO}_2$ , and an ideal gas. Below approximately 500 m depth,  $\text{CH}_4$  forms hydrate and  $\text{CO}_2$  is in liquid phase for this temperature profile.  $Z$  for  $\text{CH}_4$  and  $\text{CO}_2$  were computed using the method by Sloan (1997). From Figure 5, it is evident that these real gases cannot be treated as an ideal gas in deepwater.

### 3.3 The effect of pressure on solubility

The solubility of gas in water is commonly calculated by the simple Henry's law given as:

$$P = Hx^l \quad (14)$$

where  $H$  = Henry's law constant, which is dependent on the water temperature;  $x^l$  = mole fraction of dissolved gas in solution, which can be easily transferred to  $C_s$ .

The applicability of Eq. (14) is limited to low pressure conditions (e.g. an ideal gas). In the case of deep water, where the pressure is high, the solubility computations can be improved by using a modified form of Henry's law (King, 1969):

$$f^g = Hx^l \exp\left(\frac{pv^l}{RT}\right) \quad (15)$$

where  $f^g$  = fugacity of gas in gas phase;  $v^l$  = partial molar volume of gas in solution.

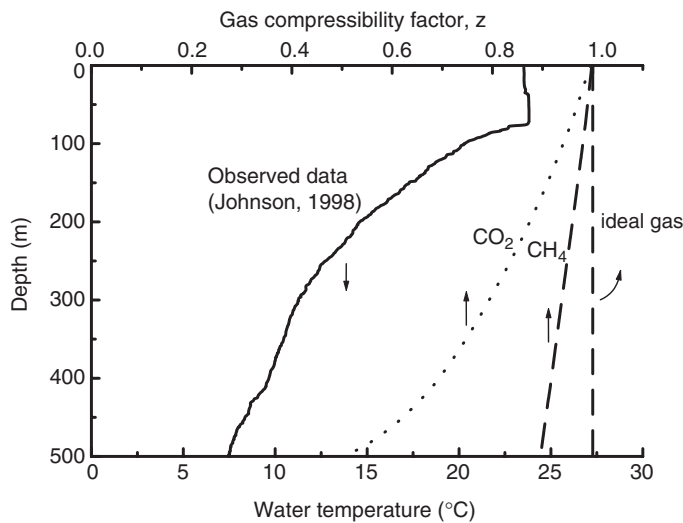


Figure 5 Water temperature profile and gas compressibility factor in the Gulf of Mexico.

Zheng and Yapa (2002) used this modified form to compute the dissolution for many cases and compare with experimental data.  $H$  and  $f^g$  were calculated by a correlation for gas in water and the Peng-Robinson equation-of-state respectively from Sloan (1997).  $v^l$  is taken to be 33 and 36.5  $\text{cm}^3/\text{mole}$  for  $\text{CO}_2$  and  $\text{CH}_4$  respectively as suggested by King (1969). Zheng and Yapa's (2002) comparisons for  $\text{CO}_2$  solubility in water at 40°C at different pressures between experimental data (King, 1969) show that Eq. (14) approximates solubility well until about 20 atm (approximate water depths of 200 m), but deviates significantly after that. Equation (15) calculates solubility well up to 200 atm (approximate water depths of 2000 m). Zheng and Yapa (2002) also made other comparisons using Eqs. (14) and (15) with experimental data. In all cases, the use of Eq. (15) provided better results. These results are not repeated here.

Figure 6 shows the comparisons between the observed and computed  $\text{CH}_4$  solubility in water using simple Henry's law (Eq. (14)) and modified Henry's law (Eq. (15)). The data are presented in 3 different blocks because they correspond to different temperatures. The available experimental data (Lekvam and Bishnoi, 1997) are such that at higher temperatures the pressure range is also higher. Nevertheless, it shows that at higher pressures the discrepancy between the experimental observations and solubility computed using simple Henry's law is larger. In fact, we can see that as the pressure increases the discrepancy grows. Therefore, at higher pressures modified Henry's law

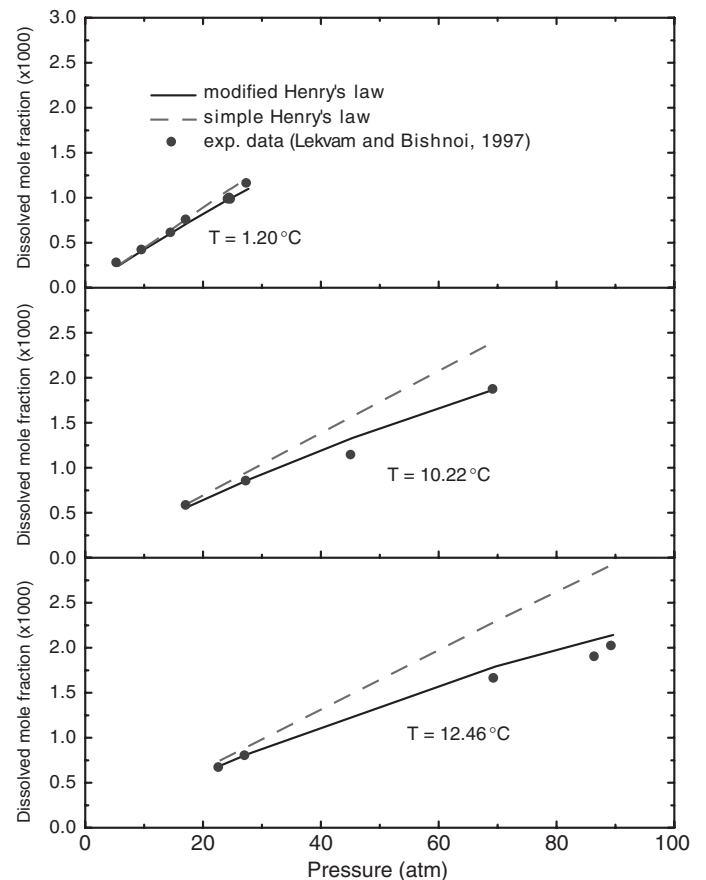


Figure 6 Comparison between computed and observed solubility of  $\text{CH}_4$  in water.

provide better computational values for solubility. The higher pressures in this plot correspond to what is expected in deepwater spills.

### 3.4 The effect of salinity on solubility

For the convenience of application, Eq. (15) is modified as follows (Weiss, 1974):

$$C_s = H^* f^s \exp\left(\frac{(1-P)v^l}{RT}\right) \quad (16)$$

where  $P$  and  $f^s$  are in atm.;  $C_s$  is in mole/m<sup>3</sup>;  $H^*$  is another form of Henry's law constant [mole/m<sup>3</sup> · atm]. Weiss (1974) and Yamamoto *et al.*'s (1976) computations showed that  $H^*$  in seawater is 15% and 20% lower than in distilled water for CO<sub>2</sub> and CH<sub>4</sub> respectively. We use the formulation given in Sloan (1997) to compute  $H$ . This formulation is more recent and has been well tested. Coefficients for this approach are available for a wider variety of gases.  $H$  is a function of temperature with multiple terms including logarithmic ones and gas constant. A correction of 20% is applied to account for the salinity effect.

### 3.5 Mass transfer coefficient of gas bubbles

According to Clift *et al.* (1978), the mass transfer coefficient of gas bubbles in liquids is dependent on the size and shape of bubbles as well as gas diffusivity in liquids. Therefore, a single formulation, such as that for rigid spheres or fluid spheres, is unable to cover the mass transfer coefficient for a broad range of bubble sizes in deepwater scenarios. Using the existing literature Zheng and Yapa (2002) presented a discussion to calculate the mass transfer coefficient for various bubble shapes. They provided comparisons between computed values and the experimental data. The method they presented covered spherical, ellipsoidal, spherical-cap ranges for bubble shapes.

## 4 Buoyant velocity of oil, gas, and hydrate particles/bubbles

In stratified ambient conditions a jet/plume may reach a neutrally buoyant level beyond which the jet/plume dynamics are no longer important. It has been observed that at this level oil is broken into small droplets and the transport beyond that could be modeled using advection-diffusion equation for oil, gas, and hydrates (Rye *et al.*, 1996; Rye and Brandvik, 1997; Yapa and Zheng, 1997; Johansen, 2000). These gas hydrates can be solid-like spherical or non-spherical particles with specific gravity in the range 0.9 ~ 0.98. In jets/plumes that consist of a mixture of oil and gas or oil and hydrate particles, a slip velocity exists between rising bubbles and the liquid within the jet/plume area. The slip velocity in a plume is considered to be the same as the terminal velocity of a bubble. Therefore, it is important to calculate the terminal velocity of bubbles of different densities and shapes for a number reasons: slip velocity of gas in the jet/plume; slip velocity of hydrates in the jet/plume; oil, gas, and hydrate particle movement in the post plume phase.

There are a large number of models that use a two equation approach to calculate the terminal velocity of a particle (solid, liquid, or gas). In this approach the terminal velocity of a particle is estimated by assuming the particle to be spherical and rigid and applying the force balance between buoyancy and drag forces. The drag coefficient  $C_D$  is approximated as an inverse function of Reynolds number  $R$  for small  $R$  values and  $C_D$  as a constant for larger  $R$  values. The resulting commonly used 2-equation approach: Stokes and Reynolds equations, has been used in many oil and gas spill models (e.g. Yapa *et al.*, 1999; Johansen, 2000).

Based on the work of Clift *et al.*, (1978), Zheng and Yapa (2000) described an integrated 8 equation approach to calculate the velocity of bubbles/droplets in a liquid. This approach accounts for the increase in drag at larger diameters. They also showed through comparison with experimental data that this integrated approach gives excellent comparison and better results than the two-equation approach for bubble/droplet velocity and covers wider range of sizes/shapes (spherical, ellipsoidal, and spherical-cap). Details of the computational method and comparisons can be found in Zheng and Yapa (2000).

## 5 The jet/plume model with integrated thermodynamics and gas hydrate kinetics

The hydrate thermodynamics, formation and decomposition kinetics, heat and mass transfer and the algorithms for rise velocity and free gas dissolution discussed in previous sections are integrated with the jet/plume hydrodynamics to form the model.

The model uses the Lagrangian integral control volume approach. A Lagrangian element is defined as a control volume (CV) moving with its local centerline velocity along the centerline of the jet/plume. The element thickness is  $h = |\mathbf{V}|\Delta t$ , in which  $h$  is the height of the CV,  $|\mathbf{V}|$  is the magnitude of the jet velocity, and  $\Delta t$  is a specified time step.  $\Delta t = 0.1b_0/|\mathbf{V}|$  was suggested by Lee and Cheung (1990), where  $b_0$  is the radius of the nozzle. The following assumptions relate to the jet/plume hydrodynamics.

In case of no gas separation, the flux of the number of bubbles,  $J$ , is equal to a constant  $J_N$  [1/s] (the flux at the nozzle), i.e. bubble coalescence is neglected. In case of gas separation,  $J$  is multiplied by a factor  $f$ .  $f$  is the fraction of gas that remains in the CV. Considering the slow hydrate decomposition rate, gas released from hydrate decomposition is assumed to dissolve into water immediately. This has been observed in limited experiments.

In the Lagrangian integral control volume method, it is the gross behavior of the plume at a cross section that is being investigated. Gas bubble size distribution inside a given CV at a given time is assumed to be uniform, but the gas bubble size can vary with CV and time. At present time there is not enough knowledge to define the gas bubble spectrum within a CV. The effects of gas bubble size are transferred to the plume behavior in the form of slip velocity of gas bubbles and the hydrate formation rate. In field experiments, the most commonly observed size range is 1 ~ 10 mm diameter (Johansen *et al.*, 2001). The larger

particles influences the plume behavior more. For gas bubbles in 5 ~ 10 mm diameter range in sea water, Zheng and Yapa (2000) showed that the slip velocity is approximately constant. Therefore, the assumptions above are reasonable.

### 5.1 Governing equations for main jet/plume

Without a strong crossflow, the gas phase is expected to occupy the inner core (Yapa and Zheng, 1997). The number of bubbles in a control volume (CV),  $N$ , is given by  $J_N h / (w + w_b)$ , where  $h$  = height of a CV;  $w$  = vertical velocity of plume liquid; and  $w_b$  = gas slip velocity.

Under strong crossflow conditions, the jet/plume will bend significantly soon after release. The slip velocity between the gas phase and liquid phase causes the gases to move to the upper boundary side in a bent jet/plume. This can cause separation of gas from the main jet/plume. The model is based on a Lagrangian frame moving with the CV and keeps updating the mass of each phase in CV. In a bent jet/plume with gas separation taken into account, the number of bubbles in a CV is  $N = (f \cdot J \cdot h) / (v_j + w_b \sin \varphi) = f \cdot J \cdot \tau$ , where  $\tau$  is the time taken for one bubble to travel through the length of the CV;  $v_j$  = the jet/plume velocity;  $\varphi$  = the angle of the jet/plume axis from the horizontal;  $f$  = a fraction that represent the gas portion left in CV,  $J$  = the number flux of bubbles. If there is no gas separation  $f = 1$ ,  $J = J_N$  = constant.  $f$ ,  $J$ , and  $\tau$  represent the change of gas mass in a CV. The following equations are applied to a CV.

#### Conservation of liquid mass

$$\frac{dm_l}{dt} = \rho_a Q_e - f \cdot J \cdot \tau \cdot n_h \frac{dn}{dt} M_w \quad (17)$$

where  $m_l$  = the liquid mass in CV [kg] =  $\rho_l \pi b^2 (1 - \beta \varepsilon) h$ ;  $\beta$  = the ratio between the cross-sectional area occupied by gas (inter-dispersed with liquid) and the cross-section area of the CV (Yapa and Zheng, 1997);  $\varepsilon$  = volume fraction of gas bubbles with hydrate shell, where  $\varepsilon = (\rho_l - \rho) / (\rho_l - \rho_{com})$ ,  $\rho_{com} = (\rho_b r_b^3 + \rho_h (r_h^3 - r_b^3)) / r_h^3$ , and  $\rho_l$ ,  $\rho$ ,  $\rho_{com}$ ,  $\rho_b$ ,  $\rho_h$ , and  $\rho_a$  = densities respectively of the liquid part of CV, gas-liquid mixture in plume, combined gas and hydrate shells, gas, hydrate, and ambient fluid [kg/m<sup>3</sup>];  $r_b$ ,  $r_h$  = the inner and outer radii of a gas bubble with a hydrate shell, if no hydrate then  $r_h = r_b$ ;  $Q_e$  = entrainment rate for ambient water [m<sup>3</sup>/s];  $n_h$  = hydrate number;  $M_w$  = molecular weight of water [kg/mol];  $dn/dt$  = hydrate formation rate for one bubble [mol/s];  $dn/dt > 0$  for hydrate formation and  $< 0$  for hydrate decomposition. The last term of the right-hand side of Eq. (17) represents the rate of loss/gain of water mass due to hydrate formation/decomposition as given by Eq. (1).

#### Loss of gas mass due to hydrate formation and free gas dissolution

$$\Delta m_b = -f \cdot J \cdot \tau \left( \frac{dn}{dt} + \frac{dn_s}{dt} \right) M_g \Delta t \quad (18)$$

in which  $\Delta m_b$  = loss of gas mass due to hydrate formation and dissolution in CV [kg] and  $m_b$  = the mass of gas in CV [kg];  $M_g$  = molecular weight of gas [kg/mol];  $dn_s/dt$  = rate of gas dissolution for one gas bubble [mol/s];  $\Delta t$  = time step [s].

#### Conservation of momentum

The momentum equations are applied to the average conditions within a CV, i.e. the distribution within the CV is ignored. However, the slip velocity between gas/hydrate and liquid is taken into account. An assumption made here is that the drag force due to the change of the flow field is not significant.

$$\frac{d}{dt} [(m_l + m_b + m_h) \cdot u] = u_a \rho_a Q_e - u \rho_{com} Q_g \quad (19)$$

$$\frac{d}{dt} [(m_l + m_b + m_h) \cdot v] = v_a \rho_a Q_e - v \rho_{com} Q_g \quad (20)$$

$$\begin{aligned} \frac{d}{dt} [m_l w + (m_b + m_h)(w + w_b)] \\ = w_a \rho_a Q_e - w \rho_{com} Q_g + (\rho_a - \rho_l) g \pi b^2 (1 - \beta \varepsilon) h \\ + (\rho_a - \rho_{com}) g \pi b^2 \beta \varepsilon h \end{aligned} \quad (21)$$

in which  $m_h$  = hydrate mass in a CV [kg];  $u$ ,  $v$ ,  $w$  = the cross sectional averaged velocity of the CV in three orthogonal directions, and  $\rho_{com}$  = the composite density of gas bubble with hydrate shell, and  $Q_g$  = the volume flux of gas (with possible hydrate shell) going out of the CV. The slip velocity,  $w_b$ , is calculated using the composite density of the gas and hydrate. The first terms on the right-hand side of Eqs. (19)–(21) represent the momentum from the entrained liquid mass. The second terms in Eqs. (19)–(21) represent the loss of momentum due to gas (in gas or hydrate form) that moves outside the jet/plume boundaries. The third term in Eq. (21) is related to the vertical force acting on the liquid part. The last term in Eq. (21) is related to the vertical force acting on the gas bubbles including hydrate shells. The simulation of gas separation effect is discussed in detail in a later section. Complete details on computing  $\beta$  and  $Q_g$  were give in Chen and Yapa (2001a).

#### Conservation of heat

$$\frac{d}{dt} [(C_{pl} m_l + C_{ph} m_h) T] = C_{pl} T_a \rho_a Q_e + f \cdot J \cdot \tau \cdot \frac{dn}{dt} \lambda \quad (22)$$

in which  $C_{pl}$ ,  $C_{ph}$  = specific heat of liquid and hydrate at constant pressure [J/kg · K];  $T$  = temperature of plume [K];  $T_a$  = temperature of ambient fluid [K];  $\lambda$  = latent heat of hydrate formation or decomposition [J/mol]. The values of parameters are listed in Appendix.

The heat content of gas in the left hand side is ignored in Eq. (22) because the contribution from this term is very small compared to the other two. The first term of the right-hand side of Eq. (22) represents the heat input from entrained water. The second term represents the change in heat energy due to gain (gained by the jet fluid) or loss in the form of latent heat during hydrate formation or decomposition contributed by the gas portion of CV.

#### Conservation of salinity and oil mass

$$\frac{d(m_l I)}{dt} = I_a \frac{dm_l}{dt} \quad (23)$$

in which  $I$  = a symbol representing salinity, S, or oil concentration by mass C (depending on the property the equation describes). Equation 23 states that the change of salinity or oil mass in the CV is due to the input contributed by the entrained mass.

### Change in gas volume

The volume of gas in the jet/plume changes due to the changes in pressure and temperature as the plume travels and dissolution. Dissolution effects were discussed earlier. The changes in gas volume due to pressure and temperature changes are modeled using Eq. (11) that also allows for non-ideal behaviour.

### Entrainment

Proper estimation of the entrainment ( $Q_e$  in Eq. (17)) is important as it impacts the fate of the jet/plume. Entrainment in jets/plumes has been the subject of many investigations. Many models used constant coefficient methods to compute entrainment. However, constant coefficient methods require varying the coefficient based on the case. A summary of the various entrainment calculations can be found elsewhere (e.g. Frick, 1984; Lee and Cheung, 1990). Lee and Cheung (1990) proposed the idea of computing the entrainment as the sum of shear-induced entrainment and forced entrainment. Forced entrainment was computed based on the ambient flow interception in the “windward” side of the buoyant jet. Lee and Cheung’s (1990) algorithm was adopted and extended to 3-D by Yapa and Zheng (1997). The comparisons between laboratory and field experiments with computer simulations using this entrainment yielded very good results (Zheng and Yapa, 1998; Yapa *et al.*, 1999). The strength of this algorithm is that there is no need to change entrainment coefficients from case to case. The same formulation is used in this paper to compute entrainment.

### 5.2 Tracking the fate and trajectories of gas bubbles

Available models do not track the fate of gas once it is outside the main plume (i.e. beyond the region where jet/plume dynamics are taken into account). If the gases are toxic or flammable we need to know the trajectories of the gas and their physical fates. Since the gases dissolve, when and where the gas will be completely dissolved is also important from a toxicological point. In this section, tracking the fate and trajectory of gases that separate from a bent plume is integrated with the model for jet/plume dynamics.

When the gas separation starts, the gas bubbles have the velocity of gas inside the CV. Once the gas bubbles are in ambient water, they will rise with the terminal velocity plus the vertical component of the ambient velocity. The terminal velocity is computed by using the algorithms given by Zheng and Yapa (2000). It is desirable to know whether it is necessary to include the dynamics of the gas bubbles during the transient period (i.e. the period during which the gas bubbles change from the velocity inside the CV to that in ambient conditions).

The focus in this section is to obtain an estimate for the transition time. Hence, the ambient turbulence is not accounted for in this analysis. Conservation of momentum for a gas bubble in an unbounded ambient flow at rest can be written as

$$m_p \frac{du_p}{dt} = -C_m m_f \frac{du_p}{dt} - C_D (\text{Re}^*) \rho_f \frac{1}{8} \pi d^2 u_p^2 - m_p g + m_f g \quad (24)$$

Table 1 Sample transient times computed from Eq. (24) for escaping gas.

$u_0$ (m/s)	$C_D$	$\text{Re}^*$	Time to reach $w_b$ (s)
0	0.5	1000	0.12
0	1.0	100	0.08
1	0.5	1000	0.12
1	1.0	100	0.08

where  $m_p = (\pi/6)\rho_p d^3$  = the mass of the gas bubble;  $m_f = (\pi/6)\rho_f d^3$  = the mass of the ambient fluid displaced by the gas bubble;  $u_p$  = gas bubble velocity;  $C_D$  = the drag coefficient (assumed constant);  $C_m$  = the added mass coefficient (=0.5 for rigid and spherical shape);  $\text{Re}^*$  = Reynolds number based on gas bubble diameter. The initial condition is  $u_p = u_0$ .

Equation 24 is numerically solved using 4th order Runge–Kutta method to find the time taken for the escaped gas to reach  $w_b$  (vertical velocity of the ambient water is generally very small). Four sample calculations are shown in Table 1, using a gas bubble size of 5 mm, density of 73 kg/m<sup>3</sup> (= CH<sub>4</sub> at a water depth of 840 m), and a temperature of 0°C.

Table 1 shows that for a typical gas bubble the time to reach  $w_b$  is very short, regardless of whether it has to accelerate ( $u_0 < w_b$ ) or decelerate ( $u_0 > w_b$ ). The added mass effect is a major factor for the short time needed for the gas to reach  $w_b$ .

After gas is separated from the plume, a Lagrangian parcel method is used to track the transport of gas, hydrate, and oil in what is called far-field conditions. The Random Walk method (Fischer *et al.*, 1979) is used to compute the diffusion. The details of advection-diffusion computations using the Lagrangian parcel method can be found in Yapa (1994). During this period the changes in mass, density, size, and the rise velocity of the gas bubbles due to changes in temperature, salinity, and pressure are calculated to account for different physical fate processes such as dissolution, hydrate formation, and decomposition. Tracking continues until the gas is dissolved or gas reach the water surface.

## 6 Modeling gas separation from a bent plume

### 6.1 Previous studies related to gas separation from a bent plume

Davidson and Pun (1999) suggested a critical height,  $Z_{sm}$  to estimate the transition point from a weakly advected plume to a strongly advected plume.

$$Z_{sm} = C_{sm} \frac{M_0^{1/2}}{u_a} \quad (25)$$

where  $M_0$  = initial momentum, and  $u_a$  = ambient velocity.  $C_{sm}$  was estimated as 1.0 by Davidson and Pun (1998). Their study did not consider the ambient density stratification.

Socolofsky (2001) developed an empirical formula to estimate the characteristic length for phase separation in multi-phase jet/plume in uniform crossflow conditions.

$$Z_{sm} = \frac{5.1B}{(u_a w_b^{2.4})^{0.88}} \quad (26)$$

where  $w_b$  = rise (or slip) velocity of a given phase (gas, oil or solid particles), and  $B$  = buoyancy flux of mixture ( $\text{m}^4/\text{s}^3$ ). The ambient density stratification is not directly included in Eq. (26) but may be indirectly represented by  $w_b$ .

The models of Yapa *et al.* (2001) and Spaulding *et al.* (2000) do not allow for the gases to separate from rising plume fluid until a neutral buoyancy level (or trap height) is reached. Johansen (2000) developed a model, DEEPBLOW, that allows the separation of gas with a “well mixed” assumption. A Lagrangian control element method was used to track the plume trajectory. Johansen (2000) assumed that the unescaped gas inside the control element was well mixed. DEEPBLOW does not track the gas bubbles once they are separated from the main plume.

Gas separates because it gradually moves to one side of the jet; therefore the “well-mixed” assumption is not consistent with the rest of the algorithms in a model that simulate gas separation. When the separation starts, the unescaped gas will move to the upper side of the CV and cannot mix well. A model that simulates gas separation with “well mixed” assumption under-estimates the speed of separation of gas and hence tend to over-estimate the terminal level of the jet/plume dynamics (TLPD) under crossflow conditions.

## 6.2 Modeling the gas separation

Before gas separation begins, gas is assumed to occupy the entire CV. Gas can escape from the main CV due to slip velocity between gas and liquid (oil/water mix). This however, is significant only if the jet/plume is sufficiently bent due to cross flow, otherwise gas moved at a different velocity ends up in a different CV, thus moving inside the plume.

A gas bubble motion inside and outside the plume can be described as follows. A gas bubble inside is assumed to move with the velocity of CV plus the vertical slip velocity  $w_b$  (the same as terminal velocity). If the gas bubble is outside the plume it moves with the ambient velocity plus  $w_b$ . Here a random component is added to simulate the turbulent diffusion, the details of which were described in Yapa (1994). As justified in the previous section the transition time from the inside velocity to the outside velocity is very small. Therefore, the velocity change is adjusted linearly over a small time step. The description above can be mathematically stated for simplicity as

$$\vec{V}_g = a\vec{V}_j + b\vec{V}_a + w_b\vec{k} \quad (27)$$

where  $a = 1$  and  $b = 0$  if the gas bubble is inside the plume;  $a = 0$  and  $b = 1$  if the gas bubble is outside the plume and after a very short transition period.  $\vec{V}_g$  = velocity of a gas bubble,  $\vec{V}_j$  = velocity of the jet, and  $\vec{V}_a$  = the velocity of ambient flow.

Two criteria are used to determine when it is possible for gas to separate from the main plume. Davidson and Pun's (1999) formula for  $Z_{sm}$  is used as a necessary criteria, i.e. no gas separation if  $z < Z_{sm}$ . Then the angle at which the gas will move immediately after escaping from the main plume is computed. If this angle (measured from a horizontal plane) is steeper than the angle of the jet, the gas is assumed to escape.

The amount of gas that can escape during a given time step  $\Delta t$  is computed as follows. The distance the gas moves relative to the liquid is  $w_b \Delta t$ . By drawing two circles (the cross sectional shape of the CV at a section), the portions overlapping and of the gas outside the main CV can be computed. The growth of the CV is computed using the governing equations described in Eqs. (17)–(23). Details of the algorithm especially the numerical implementation are given in Chen and Yapa (2001a).

The model assumes that the space occupied by gas (this is an area of gas/fluid mix at a cross section in CV) expands at the same expansion rate as the overall jet/plume of CV, preserving the shape (part of a circle); hence the gas volume fraction ( $\varepsilon$ ) in gas portion may decrease (dilute) due to turbulent entrainment.

## 6.3 Comparison of gas separation simulation with experimental data

### Experimental setup

Experimental data on gas separation from an oil/gas plume are limited. Socolofsky *et al.* (1999) and Socolofsky (2001) conducted experiments to investigate the behavior of oil/gas plumes in a cross-flow. The experiments consisted of 3 oil flow rates (from 250 to 1000 mL/min) and 4 air flow rates (from 250 to 2500 mL/min). The experiments cover relatively weak (2 cm/s) to strong cross flow (10 cm/s). The gas to oil ratio (GOR) varied from 1 to 10.

### Comparisons

Using the independent variables of the experiments as input, CDOG simulated the experiments. Experimental observations were available in the form of video images. Therefore, the nature of the comparison is qualitative. Sample comparisons between the model simulations and experimental observations are shown in Figure 7a, b, and c. In these figures, the solid lines and the dashed/dotted line show the simulated plume boundaries and the centerline respectively. The dashed lines show the observed plume boundaries. The scattered circles represent the simulated escaped gas bubbles. The size of the bubbles do not represent a scale. The dashed line near the escaped gas is the observed gas trajectory. Complete comparisons are in Chen and Yapa (2001a).

The experiments and simulations show that the increase in cross current increases the chance of separation by lowering the point where separation starts. The volumes of gas shown outside the plume are similar between the experiments and simulations. The separation points and the volumes are consistent between the simulations and the observations. Overall, the trends shown in experiments are well captured by the numerical model. No tuning coefficients varied from case to case in these simulations.

## 7 Summary

In this paper, a comprehensive three-dimensional numerical model has been developed to simulate the behaviour of oil and gas blowouts from deepwater. The model is based on the Lagrangian integral concept. It simulates the phase changes of gas that can

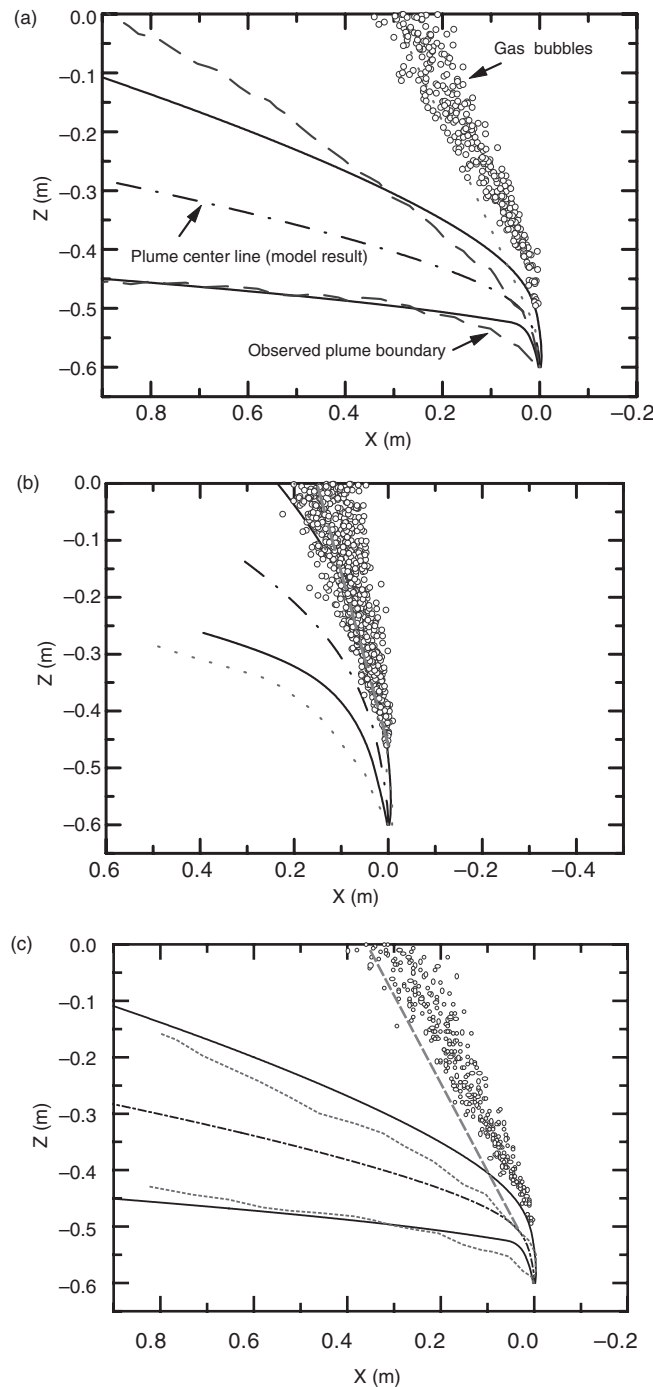


Figure 7 Comparison of gas separation from an oil/gas plume in a cross flow – numerical simulation: CDOG model; experimental data from Socolofsky *et al.*, (1999). (a) case C15; (b) case C4; (c) case C5.

occur in deepwater, associated thermodynamics, and its impact on the hydrodynamics of the jet/plume. Phase changes of gas consists of hydrate formation and decomposition. In simulating these, the model considers both thermodynamics and kinetics of hydrate formation and decomposition. The model accounts for gas dissolution and the non-ideal behaviour of gasses in high-pressure conditions.

The CDOG model presented can take into account the complete three-dimensional variation in ambient velocity, temperature, and salinity. Ambient velocity variations are used for entrainment calculations, jet/plume hydrodynamical equations, and computing the far-field movement of oil and gas. Ambient

temperature and salinity variations are taken into account in computing the ambient density stratification. Furthermore, the ambient temperature also affects the jet/plume thermodynamics and gas phase changes and dissolution. The model considers possible gas separation when a jet/plume is in the presence of a relatively strong ambient current.

Each module has been compared with experimental data, subject to the availability. In all cases the comparisons between the numerical simulation and the observed data are good. For some modules, summary results from comparisons are presented here while for the details the reader is referred to separate publications to keep the paper length under control. The comprehensive model

CDOG has been used for comparing the large scale and unique field experiments conducted mainly to support this model. These results will be presented in the companion paper (part II).

### Acknowledgements

This study was supported by the Minerals Management Service (MMS) of the U.S. Department of the Interior. The authors acknowledge the support of Robert LaBelle and Walter Johnson of the MMS, Dan Allen, Cortis Cooper, and Timothy Finnigan of Chevron, USA and the members of the Deep Spill Task Force (DSTF) for this work. The authors would like to thank Dr. Eric Adams and Scott Socolofsky at MIT for their help and permission of using their experimental data. The paper represents the views of the authors and not the MMS or DSTF.

### Appendix: A table of model parameters

Table A1 Parameters used in the simulations.

Parameters	Unit	Notation	Value	References
Specific heat of water at constant pressure	[J/kg · K]	$C_{pl}$	4216.3	Jamaludin, 1991
Specific heat of CH <sub>4</sub> hydrate at constant pressure	[J/kg · K]	$C_{ph}$	2010	Selim and Sloan, 1985
Latent heat of CH <sub>4</sub> hydrate formation/decomposition	[J/mol]	$\lambda$	62800	Jamaludin, 1991
Typical CH <sub>4</sub> hydrate density	[kg/m <sup>3</sup> ]	$\rho_h$	900	Johansen, 2000; Sloan, 1997

### References

1. BARBOSA, Jr. J.R., BRADBURY, L.J.S. and SILVA FREIRE, A.P. (1996). "On the Numerical Calculation of Bubble Plumes, Including an Experimental Investigation of its Mean Properties", presented at the 1996 Society of Petroleum Engineers (SPE) Eastern Regional Meeting, Columbus, Ohio, October 23–25.
2. BISHNOI, P.R. and NATARAJAN, V. (1996). "Formation and Decomposition of Gas Hydrate", *Fluid Phase Equilibria*, 117, 168–177.
3. BREWER, P.G., ORR, Jr. F.M., FRIEDERICH, G., KVENVOLDEN, K. A. and ORANGE, D.L. (1998). "Gas Hydrate Formation in the Deep Sea: In situ Experiments with Controlled Release of Methane, Natural Gas, and Carbon Dioxide", *Energy & Fuels*, 12(1), 183–188.
4. CHEN, F.H. and YAPA, P.D. (2001a). "Modeling Gas Separation from a Bent Oil and Gas Jet/plume", *Proceedings, International Marine Environmental Modelling Seminar (IMEMS) Conference*, New Orleans, LA, October.
5. CHEN, F.H. and YAPA, P.D. (2001b). "Estimating Hydrate Formation and Decomposition of Gases Released in a Deepwater Ocean Plume", *J. Marine Systems*, 30, 21–32.
6. CHEN, F.H. and YAPA, P.D. (2003). "A Model for Simulating Deepwater Oil and Gas Blowouts – Part II: Comparison of Numerical Simulations with 'Deepspill' Field Experiments", *J. Hydra. Res.*, IAHR, 41(4), 353–365.
7. CLIFT, R., GRACE, J.R. and WEBER, M.E. (1978). *Bubbles, Drops, and Particles*. Academic Press, New York.
8. COOPER, C., FORRISTALL, G.Z. and JOYCE, T.M. (1990). "Velocity and Hydrographic Structure of Two Gulf of Mexico Warm-Core Rings", *J. Geophys. Res.*, 95(C2), 1663–1679.
9. DAVIDSON, M.J. and PUN, K.L. (1998). "A Hybrid Model for the Prediction of Initial Dilutions from Outfall Discharge", *J. Hydr. Engrg.* ASCE., 124(12), 1188–1197.
10. DAVIDSON, M.J. and PUN, K.L. (1999). "Weakly Advected Jets in Cross-flow", *J. Hydr. Engrg.* ASCE., 125(1), 47–58.
11. DHOLABHAI, P.D., KALOGERAKIS, N. and BISHNOI, P.R. (1993). "Kinetics of Methane Hydrate Formation in Aqueous Electrolyte Solutions", *The Canadian J. Chemical Engrg.*, 71(2), 68–74.
12. DRANGE, H. and HAUGAN, P.M. (1992). "Carbon Dioxide Sequestration in the Ocean: The Possibility of Injection in Shallow Water", *Energy Conversion and Management*, 33(5–8), 697–704.
13. ENGLEZOS, P., KALOGERAKIS, N., DHOLABHAI, P.D., BISHNOI, P.R. (1987a). "Kinetics of Formation of Methane and Ethane Gas Hydrates", *Chem. Engrg. Sci.*, 42(11), 2647–2658.
14. ENGLEZOS, P., KALOGERAKIS, N., DHOLABHAI, P.D., BISHNOI, P.R. (1987b). "Kinetics of Gas Hydrates Formation from Mixtures of Methane and Ethane", *Chem. Engrg. Sci.*, 42(11), 2659–2666.
15. FISCHER, H.B., LIST, E.J., KOH, R.C.Y., IMGERGER, J. and BROOKS, N.H. (1979). *Mixing in Island and Coastal Waters*. Academic Press, New York, NY.
16. FRICK, W.E. (1984). "Non-empirical Closure of the Plume Equations", *Atmos. Environ.*, 18(4), 653–662.
17. GUMEROV, N.A. and CHAHINE, G.L. (1998). "Dynamics of Bubbles in Conditions of Gas Hydrate Formation", *Proceedings of the 8th International Offshore and Polar Engineering Conference*, Montreal, Canada, May 24–29.
18. HOLDER, G.D., ZETTS, S.P. and PRADHAN, N. (1988). "Phase Behavior in Systems Containing Clathrate Hydrate, A Review", *Reviews in Chem. Engrg.*, 5(1–4), 1–70.
19. JAMALUDDIN, A.K.M., KALOGERAKIS, N. and BISHNOI, P.R. (1991). "Hydrate Plugging Problems in Undersea Natural Gas Pipelines Under Shutdown Conditions", *J. Petroleum Science and Engrg.*, 5, 323–335.
20. JOHANSEN, O. (2000). "DeepBlow – a Lagrangian Plume Model for Deep Water Blowouts", *Spill Science & Technology Bulletin*, 6, 103–111.
21. JOHANSEN, O., RYE, H., MELBYE, A., JENSEN, H., SERIGSTAD, B. and KNUTSEN, T. (2001) "Deep Spill JIP Experimental Discharges of Gas and Oil at Helland Hansen,

- Parts I, II, and III – Technical Report*, SINTEF Applied Chemistry, Norway.
22. JOHNSON, W. (1998). Data for Gulf of Mexico, US Minerals Management service (MMS), Herndon, VA, Personal Communications.
  23. KIM, H.C., BISHNOI, P.R., HEIDEMANN, R. A. and RIZVI, S.S.H. (1987). “Kinetics of Methane Hydrate Decomposition”, *Chem. Engrg. Sci.*, 42(7), 1645–1653.
  24. KING, M.B. (1969). *Phase Equilibrium in Mixtures*, Pergamon Press, Oxford.
  25. LANE, J.S. and LABELLE, R.P. (2000). “Meeting the Challenge of Potential Deepwater Spills: Cooperative Research Effort Between Industry and Government”, *Proc. Society of Petroleum Engineers Conference Slavenger*, Norway, 26–28 June.
  26. LEE, J.H.W. and CHEUNG, V. (1990). “Generalized Lagrangian Model for Buoyant Jets in Current”, *J. Environ. Engrg. ASCE.*, 116(6), 1085–1106.
  27. LEKVAM, K. and BISHNOI, P.R. (1997). “Dissolution of Methane in Water at Low Temperature and Intermediate Pressures”, *Fluid Phase Equilibrium*, 131, 297–309.
  28. LIRO, C.R., ADAMS, E.E. and HERZOG, H.J. (1992). “Modeling the Release of CO<sub>2</sub> in the Deep Ocean”, *Energy Conversion and Management*, 33(5–8), 667–674.
  29. MAINI, B.B. and BISHNOI, P.R. (1981). “Experimental Investigation of Hydrate Formation Behaviour of a Natural Gas Bubble in a Simulated Deep Sea Environment”, *Chem. Engrg. Sci.*, 36, 183–189.
  30. RYE, H., BRANDVIK, P.J. and REED, M. (1996). “Subsurface Oil Release Field Experiment-observations and Modelling of Subsurface Plume Behavior”, *Proceedings, 19th Arctic and Marine Oil Spill Program (AMOP) Technical Seminar*, 2, 1417–1435.
  31. RYE, H., BRANDVIK, P.J. and STORM, T. (1997). “Sub Surface Blowouts: Results from Field Experiments”, *Spill Science and Technology Bulletin*, 4(4), 239–256.
  32. RYE, H. and BRANDVIK, P.J. (1997). “Verification of Subsurface Oil Spill Models”, *Proceedings, 1997 International Oil Spill Conference*, Fort Lauderdale, Florida, 551–557.
  33. SELIM, M.S. and SLOAN, E.D. (1985). “Modeling of the Dissociation of an In-Situ Hydrate”, *Proceedings 55th Annual California Regional Meeting* March 27–29, 1985, Bakersfield, California.
  34. SLOAN, E.D. (1997). *Clathrate Hydrates of Natural Gases*, Marcel Dekker, Inc., New York.
  35. SOCOLOFSKY, S.A., LEOS-URBEL, A. and ADAMS, E.E. (1999) “Draft Final Report: Exploratory Experiments with Droplet Plumes in a cross-flow”, *Final Report: Experimental Study Of Multi-Phase Plumes to the Minerals Management Service, No. 1435-01-98-CT-30964*.
  36. SOCOLOFSKY, S.A. (2001). “Laboratory Experiments of Multi-phase Plumes in Stratification and Crossflow”, Ph.D. Thesis, Massachusetts Institute of Technology, MA, 1–233.
  37. SPAULDING, M.L., BISHNOI, P.R., ANDERSON, E. and ISAJI, T. (2000). “An Integrated Model for Prediction of Oil Transport from a Deep Water Blowout”, *23rd AMOP Technical Seminar 2000*, June 14–16, 2000, Vancouver, British Columbia, Canada. Vol. 2, 611–635.
  38. TOPHAM, D.R. (1984a). “The Formation of Gas Hydrates on Bubbles of Hydrocarbon Gases Rising in Seawater”, *Chem. Engrg. Sci.*, 39(5), 821–828.
  39. TOPHAM, D.R. (1984b). “The Modelling of Hydrocarbon Bubble Plumes to Include Gas Hydrate Formation”, *Chem. Engrg. Sci.*, 39(11), 1613–1622.
  40. VYSNIAUSKAS, A. and BISHNOI, P.R. (1983). “A Kinetic Study of Methane Hydrate Formation”, *Chem. Engrg. Sci.*, 38(7), 1061–1072.
  41. WEISS, R.F. (1974). “Carbon Dioxide in Water and Seawater: The Solubility of a Non-ideal Gas”, *Marine Chemistry*, 2, 203–215.
  42. WUEST, A., BROOKS, N.H. and IMBODEN, D.M. (1992). “Bubble Plume Modeling for Lake Restoration”, *Water Resources Research*, 28(12), 3235–3250.
  43. YAMAMOTO, S., ALCAUSKAS, J.B. and CROZIER, T.E. (1976). “Solubility of Methane in Distilled Water and Seawater”, *J. Chem. Engrg. Data*, 21(1), 78–80.
  44. YAPA, P.D. (1994). “Oil Spill Processes and Model Development”, *J. Advanced Marine Technology*, AMTEC, Japan, March, 1–22.
  45. YAPA, P.D. and ZHENG, L. (1997). “Simulation of Oil Spills from Underwater Accidents I: Model Development”, *J. Hydr. Res. IAHR*, 35(5), 673–687.
  46. YAPA, P.D., ZHENG, L. and NAKATA, K. (1999). “Modeling Underwater Oil/Gas Jets and Plumes”, *J. Hydr. Engrg. ASCE*, 125(5), 481–491.
  47. YAPA, P.D., ZHENG, L. and CHEN, F.H. (2001). “A Model for Deepwater Oil/Gas Blowouts”, *Marine Pollution Bulletin, (The Inter. J. Marine Environmental Scientists/Engineers)*, Elsevier Science Publications, UK, 43, 234–241.
  48. ZHENG, L. and YAPA, P.D. (1998). “Simulation of Oil Spills from Underwater Accidents II: Model Verification”, *J. Hydr. Res. IAHR*, 117–134.
  49. ZHENG, L. and YAPA, P.D. (2000). “Buoyant Velocity of Spherical and Non-spherical Bubbles/Droplets”, *J. Hydr. Engrg. ASCE*, 852–854.
  50. ZHENG, L. and YAPA, P.D. (2002). “Modeling Gas Dissolution in Deepwater Oil/Gas Spills”, *J. Marine Systems*, 31(4), 299–309.

